CrystEngComm

Accepted Manuscript

ROYAL SOCIETY OF CHEMISTRY

www.rsc.org/crystengcomm

Graphic Abstract for:

The effect of terminal dimethyl and diethyl substituents on the J-aggregate-like molecular arrangement of bisazomethine dye molecules

Takumi Jindo, Byung-Soon Kim, Naho Sasaki, Yohei Shinohara, Young-A Son, Sung-Hoon Kim and Shinya Matsumoto*

*Corresponding author. Tel.: +81-45-339-3366; Fax: +81-45-339-3345. *E-mail address:* smatsu@ynu.ac.jp (Shinya Matsumoto).

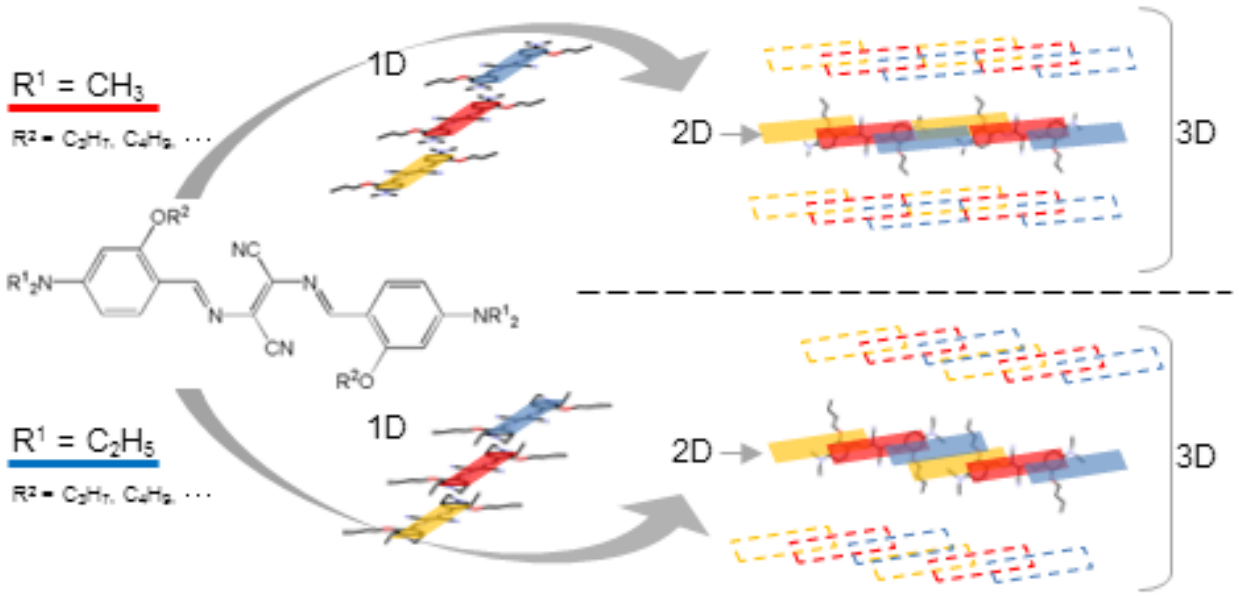

The terminal dimethyl and diethyl substituents of the bisazomethine derivatives did not affect the 1-D arrangements of the π-π stacking molecules in the crystalline states of this dye system. However, the terminal dialkyl substituents did affect the arrangement of the molecules aligned along the long molecular axes and the short molecular axes, leading to the different structural features of the J-aggregate like 2-D molecular arrangements and the 3-D crystal structures of the derivatives.

The effect of terminal dimethyl and diethyl substituents on the J-aggregate-like molecular arrangement of bisazomethine dye molecules

Takumi Jindo[a], Byung-Soon Kim[a], Naho Sasaki[a], Yohei Shinohara[a], Young-A Son[b], Sung-Hoon Kim[c,d] and Shinya Matsumoto[a,*]

[a]*Graduate School of Environmental and Information Sciences, Yokohama National University, 79-7, Tokiwadai, Hodogaya-ku, Yokohama 240-8501, Japan.*
[b]*School of Chemical and Biological Engineering, Chungnam National University, Daejeon 305-764, Korea.*
[c]*Department of Textile System Engineering, Kyungpook National University, Daegu 702-701, Korea.*
[d]*School of Chemical Science & Technology, Zhanjiang National University, Zhanjiang 524048, PR China.*

Abstract

Derivatives of 2,3-bis[(*E*)-4-(diethylamino)-2-alkoxybenzylideneamino]fumaronitrile (DEA) form J-aggregate-like 2-dimensional (2-D) arrangements of π–π-stacked molecules in the solid state. The structural features of the 2-D molecular arrangements were controlled by the alkoxy substituents of the DEA derivatives. In this study, single crystal structures of the six 2,3-bis[(*E*)-4-(dimethylamino)-2-alkoxybenzylideneamino]fumaronitrile (DMA) derivatives are reported, five of which formed J-aggregate-like 2-D molecular arrangements in the solid state. The molecular arrangements of four of the six DMA derivatives were geometrically compared with those of the corresponding four DEA derivatives, to evaluate the effect of the terminal dimethyl and diethyl substituents on the J-aggregate-like 2-D molecular arrangement. Lattice energy calculations were also carried out to interpret the effects of the terminal dialkyl substituents on the crystal structures from an energetic perspective. The dialkyl substituents of the selected DMA and DEA derivatives did not influence the formation of 1-D π–π stacking motifs. However, the location of the terminal dialkyl substituents influenced the spacing between molecules aligned along the long axis and this was found to be key in determining the formation of J-aggregate-like 2-D arrangements.

Keywords

bisazomethine dyes, J-aggregates, crystal structure, substitution effects, lattice energy calculation

*Corresponding author. Tel.: +81-45-339-3366; Fax: +81-45-339-3345. *E-mail address:* smatsu@ynu.ac.jp (Shinya Matsumoto).

1. Introduction

J-aggregates are known as low-dimensional aggregates of molecules.[1–18] They exhibit a characteristic narrow and intense visible absorption band at longer wavelengths,[2] a large optical nonlinearity[3–5] and ultrafast photoexcitation decay[6] that is attributed to intermolecular interactions in certain arrangement of molecules.[7–18] Because of these optical properties, J-aggregates are attracting increasing attention as candidates to improve the functionality of organic optoelectronic devices.

A non-ionic bisazomethine dye, *N*,*N*'-bis[4-(*N*,*N*-diethylamino)benzylidene]diaminomaleonitrile (DE2), derived from diaminomaleonitrile and 4-diethylaminobenzaldehyde has been reported to exhibit a J-aggregate-like narrow and intense absorption band at around 650 nm in vapour-deposited films.[19] DE2 films also show good emission characteristics[20] and an enhancement in the third-order non-linear optical response[21,22] due to the J-aggregates formed in the solid state. Possible applications of these films include organic semiconductors and field-effect transistors.[23–26] However, these DE2 films also include non-aggregated solid phases, and these are responsible for the broad absorptions seen at shorter wavelengths.[27] In order to solve this problem, novel bisazomethine dyes have been synthesised[28–31] based on the reported crystal structures of DE2 and other bisazomethine dyes[32–35] and the proposed structural models of J-aggregates.[2,7–10,14] The optical properties[28,29,31] and the solid-state structures[29,30] of the novel bisazomethine derivatives have been investigated to try to develop purer J-aggregates.

2,3-bis[(*E*)-4-(diethylamino)-2-alkoxybenzylideneamino]fumaronitrile (DEA) are alkoxylated derivatives of DE2. The DEA derivatives show J-aggregate-like bathochromic absorption shifts between the solution state and solid state, for example, in vapour deposited films.[28] Crystal structures of the dye molecules show that they form J-aggregate-like two-dimensional (2-D) stacked layers.[30,35] The features of the crystal structures of the nine reported DEA derivatives are schematically summarised in Figure 1. Within the 2-D layers that are formed, the molecules are stacked with two different types of small slip angles along the long molecular axes.[30,35] As shown in Figure 1(b), the stacked molecules form a staircase-like arrangement in the 2-D layers. The 2-D molecular arrangements of the DEA derivatives are similar to the proposed 2-D molecular arrangements of J-aggregates.[8–10,14] The 2-D layers of the DEA derivatives are aligned along the short molecular axes to form the 3-D crystal structure. The interlayer separation between the adjacent 2-D layers is controlled by the alkoxy substituents. Figure 1(c) shows that larger alkoxy substituents lead to a greater interlayer separation. The alkoxy groups are parallel to the molecular π-planes. However, the larger decyloxyl substituents project out of the π-plane; this leads to a dislocation of the π–π stacking in the short molecular axis, and consequently small interlayer separations (Figure 1(d))[30] The 3-D crystal structures of the DEA derivatives are clearly partitioned into two parts. One part corresponds to the 2-D π–π stacking molecular layer. The other part consists of the flexible alkyl substituents. This two part structural feature in the solid state is also regarded as one of the promising structural motifs in spin-coated organic semiconductors that could contribute to realization of high performance organic field-effect transistors[36] and organic flexible devices[37]. The 2-D molecular arrangement of the DE2 derivatives and the effects of the substituents on this arrangement is an intriguing research area for the discussion of possible molecular designs for organic optoelectronic devices.

In this study, single crystal structures of 2,3-bis[(E)-4-(dimethylamino)-2-alkoxybenzylideneamino]fumaronitrile (DMA) were investigated. All of these derivatives have dimethyl substituents on the terminal amino group. The

chemical structure of the six DMA derivatives, **1a**–**1f**, are shown in Figure 2. Bathochromic absorption shifts in vapour deposited films of **1a**–**1f** have been reported.[28] The single crystal X-ray structures of **1a**–**1f** indicate that the J-aggregate-like 2-D molecular stacking layers formed in **1b**–**1f**, but **1a** did not form these 2-D layers. A dislocation of the π-π stacked molecules along the short molecular axes was found in the 2-D layers of **1b**–**1f**, this is similar to that of the DEA derivatives with decyloxy substituents.[30] In order to systematically evaluate the effects of the terminal dimethyl and diethyl substituents on the J-aggregate-like 2-D molecular arrangements, the four crystal structures of **1c**–**1f** were geometrically compared to the four reported crystal structures of the corresponding DEA derivatives, **2c**–**2f**. The lattice energies were also calculated for **1c**–**1f** and **2c**–**2f** to interpret the substitution effects from an energetic perspective. Effects of alkyl substitutions of organic small molecules on crystal structures are a very important topic in the field of crystal engineering. Our systematic investigation refers to the effect of the slight differences of the length of the terminal dialkyl substituents on the supramolecular arrangement of the molecules. This can guide the molecular design of bisazomethine dyes.[19–35] Also, the relationship between substitution and the bulk structure can be extended to design organic compounds used in semiconductors.[36–38]

[Figure 1]

[Figure 2]

2. Experimental

The six DMA derivatives, **1a**–**1f**, are derived from the reaction of diaminomaleonitrile with 4-(dimethylamino)benzaldehyde.[28] They were synthesised and characterised by conventional analytical methods.[28] The syntheses, solution and solid-state optical properties, and the electronic states of **1a**–**1f** are reported elsewhere.[28,31]

The syntheses, crystal structures, solution and solid-state optical properties, and the electronic states of **2c**–**2f**,[28,35] and also lattice energy calculations, for **2c**, **2e** and **2f**, [30] have been reported. The published crystal structures of **2c**–**2f** and the results of lattice energy calculations of **2c**, **2e** and **2f**, are quoted and included in some figures and tables for completeness. These published data regarding crystal structures of **2c**–**2f** are introduced to this work to systematically interpret the effects of the terminal dimethyl and diethyl substituents on the J-aggregate-like 2-D molecular arrangements.

2.1. Crystal growth and data collection

The purple (**1a**–**1e**) and reddish-purple (**1f**) single crystals were grown by solvent diffusion. Dichloroethane, dichloromethane and chloroform were used as the good solvent for **1a** and **1f**, **1b**–**1d** and **1e**, respectively. For **1a**–**1e** *n*-hexane was used as a poor solvent, and for **1f** diethyl ether was used as a poor solvent. Among the six compounds, **1a** is only crystallised concomitantly with its solvate crystals. The homogenous crystals of **1a** are thin needles and normally have low crystallinity.

The diffraction data of **1a**–**1e** were collected at room temperature (298 K) on a Rigaku R-AXIS RAPID with an image plate area detector using graphite monochromated CuK_α radiation (λ = 1.54187 Å) at 40 kV and 30 mA. The

diffraction data of **1f** was measured on the same method. However, the refinement using the reflections did not converge well, despite long collection times and re-measurements on the same method. Therefore, the diffraction data of **1f** was re-measured at low temperature (93 K) on a Rigaku XtaLAB P200 with a hybrid pixel array detector using multi-layer mirror monochromated CuK_α radiation (λ = 1.54187 Å) at 40 kV and 30 mA. Finally, the refinement in **1f** fully converged.

The structures were solved by direct methods using *SIR2004*[39] for **1b**, **1d** and **1e** and *SHELXT*[40] for **1a**, **1c** and **1f** and refined by full-matrix least-squares against F^2. All non-hydrogen atoms were refined anisotropically. The positions of all hydrogen atoms were calculated geometrically and were refined by the riding model. All calculations were performed using the CrystalStructure crystallographic software packages.[41,42] The final R-factors and structure refinement parameters for **1a**–**1f** are given in Table 1 together with the published data of **2c**–**2f**. The crystal structures of **1a**–**1f** and **2c**–**2f** were visualised and evaluated using Mercury 3.5.[43]

[Table 1]

2.2. Lattice energy calculations

Lattice energy calculations were performed by using the ZipOpec[44] module of the OPiX program package.[45] This module calculates the total lattice energy using the unit cell parameters, space group, and atomic coordinates. The positions of hydrogen atoms were normalised to the standard values of a C–H bond length (1.08 Å) and R–CH bond angles (120° and 109.5° corresponding to the bond angles of sp^2 and sp^3 hybridised orbitals of the adjacent carbon atom, respectively) estimated from the results of neutron-diffraction.[46] An empirical atom-atom potential method (UNI force field[47]) was applied in the calculations.[48,49]

3. Results and discussion

3.1. Crystal structures of the DMA derivatives

The crystallographic data for **1a**–**1f** are listed in Table 1. Among the six DMA derivatives, **1a** crystallised in the monoclinic crystal system, whereas the crystal structures of **1b**–**1f** crystallised in the triclinic crystal system. There was no similarity found between the lattice parameters of **1a**–**1f**.

Ellipsoid plots of the DMA derivatives **1a**, **1c**, **1e** and **1f** are shown in Figure 3. Bond angles, distances and the deviations of the atoms from the molecular π-planes of **1a–1f** were measured. These data are provided in the supporting information.

The DMA molecules in **1a**–**1f** sit on an inversion centre, half of the molecule comprising the asymmetric unit (Z' = 0.5). An almost identical planar geometry of the π-conjugated systems was found in **1a**–**1f**, shown in Figures S1 and S2, and Table S1. The π-conjugated systems in **1a**–**1f** had similar intramolecular bond angles and bond distances (Figure S3 and Table S2). These geometrical features are similar to the DEA derivatives reported previously,[30,35] as shown in Table S2.

The terminal dimethyl groups of **1a**–**1f** were parallel to the molecular π-planes, as shown in Table S1. Two distinct geometries of the alkoxy substituents relative to the π-planes were observed. In **1b**, **1c** and **1f** they were parallel,

and in **1a**, **1d** and **1e** they projected out from the π-planes. In the latter type, the largest deviation of the carbon atoms of the alkoxy substituents from the π-planes was more than 1 Å, as shown in Table S1. As discussed in our previous work,[30] the geometries of the alkoxy substituents of the DEA derivatives depends on the size of the alkoxy substituents. The substituents are parallel to the molecular π-plane for alkyl lengths of 2–8 and for the phenoxy substituent, but the decyloxy and benzoxy substituents project out of the π-plane.[30] In contrast, for **1a**–**1f**, the size of the alkoxy substituent did not correlate with its geometry. Molecular conformation in solid states should minimize cavities and the total lattice energies in solid state.[50-52] Thus, the differences in alkoxy geometry lead to differences in crystal packing.

[Figure 3]

The crystal structures of **1a**, **1c**, **1e** and **1f** are shown in Figures 4–7, respectively. Among the structures **1a**–**1f**, **1a** was the only one that crystallised in the monoclinic crystal system, and formed a herringbone arrangement of DMA molecules (Figure 4). In the crystal structure of **1a**, the dye molecules are π-π stacked in the [010] direction; the molecules have an intermolecular slip angle of 26° along the long molecular axis. In this dye system, a large transition dipole moment, corresponding to an intense visible absorption, is known to lie on a line aligned along its long molecular axes.[28,31] According to the theory of excitonic interactions, small slip angles between transition dipoles of molecules are an important feature of J-aggregates.[14] The small slip angle between the π–π stacking molecules in the 1-D arrangement of **1a** satisfies the one of the geometrical requirements of J-aggregates. However, the J-aggregate-like 2-D staircase molecular arrangement that is observed in the crystal structures of the DEA derivatives[30,35] was not formed in the crystal structure of **1a**.

[Figure 4]

In the triclinic crystal structures of **1b**–**1f**, J-aggregate-like 2-D molecular stacking layers were observed. The 2-D layers were found to lie on the (202) plane in **1b**, the (010) plane in **1c**, the (01-1) plane in **1d**, the (001) plane in **1e** and the (01-1) plane in **1f**. The staircase molecular arrangements in the 2-D layers of **1c**, **1e** and **1f** are shown in Figures 5(a), 6(a) and 7(a), respectively. Within the 2-D layers of **1b**–**1e**, the molecules were stacked with two types of intermolecular slip angles along the long molecular axes. These two types of small slip angles were 26° and 13° in **1b**, 26° and 14° in **1c**, 26° and 13° in **1d**, 25° and 13° in **1e**. In the 2-D layers of **1f**, the molecules were stacked toward the [100] direction with a small slip angle of 26° along the long molecular axis. The molecules aligned along the [311] direction are located in such a position to produce the 2-D staircase arrangement with the small slip angle of 9° along the long molecular axis, while the molecules aligned along the [311] direction did not overlap with each other. These two types of small slip angles between molecules in **1b**–**1f** satisfy one of the geometrical requirements for J-aggregates.[14] Therefore, we considered that the 2-D layers formed in **1b**–**1f** were potential J-aggregate structural units. Our theoretical investigation, based on excitonic interactions, has confirmed that the stacked arrangement in the 2-D layers affects the bathochromic shift observed between the solution and solid state of structures **1b**–**1f**.[31]

In **1b**–**1f**, the 3-D crystal structure is composed of 2-D layers aligned parallel to the short molecular axis. The 3-D crystal structures of **1c**, **1e** and **1f** are shown in Figures 5(b) and 5(c), 6(b) and 6(c), and 7(b) and 7(c), respectively. The interlayer distances between the adjacent 2-D layers of **1b**–**1f** are listed in Table 2. The alkoxy substituents of **1b**–**1e** are located in the interlayer spaces between the adjacent parallel 2-D layers and increase the interlayer separation. Butoxy substituents in **1d** decrease the interlayer separation, relative to **1c**, because they project out of the π-plane. In contrast, **1e**, which has pentoxy substituents, has the largest interlayer separation regardless of the projection of the substituents out of the π-plane. The decyloxy substituents, which are the longest, are arranged parallel to the π-plane and penetrate into the adjacent 2-D layers. Thus, the interlayer distance in **1f** is shorter than in **1c**–**1e**. Figure 7(c) shows the 2-D layers formed in **1f**.

Figures 5(b), 6(b) and 7(b) show the 2-D layers of **1b**–**1f** viewed along the long molecular axis. The π-π stacked molecules are slipped along the short molecular axis. This slip dislocation is similar to that in decyloxylated-DEA derivative we previously investigated[30] and that is shown in Figure 1(d). In the other DEA derivatives, the stacked molecules in the 2-D layers were almost normal to the molecular π-plane,[30,35] shown in Figure 1(c). The slip-distortion, important for the formation of J-aggregate-like 2-D arrangements, seen in structures **1b**–**1f** could be due to the presence of terminal dimethyl substituents.

[Figure 5]

[Figure 6]

[Figure 7]

[Table 2]

3.2. Geometrical comparison between the molecular arrangements of the DMA and the DEA derivatives

The molecular geometries of **1c**–**1f** were compared with the DEA derivatives, **2c**–**2f**. Both sets contain the same alkoxy substituents allowing us to evaluate the effect of the terminal dimethyl and diethyl substituents on the formation of the J-aggregates-like system. **1a** was excluded, as it did not form a 2-D arrangement in the solid state. **1b** was excluded because the X-ray crystal structure of the corresponding DEA derivative has not been solved due to the low single crystal quality.

1c–**1f**, **2c** and **2f** crystallised in *P* -1. **2d** and **2e** crystallised in the monoclinic crystal system; **2d** in $P2_1/c$ and **2e** in the non-standard $P2_1/a$ setting (Table 1). There are no similarities in the lattice parameters of **1c**–**1f** and **2c**–**2f**. All of the crystal structures were centrosymmetric, and the dye molecules were located on an inversion centre (Z' = 0.5). An almost identical planar π-conjugation was found in the crystal structures of **1c**–**1f** and **2c**–**2f**, as shown in Tables S1 and S2. Therefore, their geometries were compared to this almost identical π-conjugated structure and the molecular axes of **1c**–**1f** and **2c**–**2f**. The geometrical parameters used to evaluate the molecular arrangements of **1c**–**1f** and **2c**–**2f** are shown in Figures 8, 9 and 10. The atomic positions of the carbon atoms depicted as C6, C8, $C6^i$ and $C8^i$ in the ORTEP diagrams, and the centroids of the π-conjugated systems were selected as the measurement standards, as shown in Figure 8. The line connecting the two C-atoms, C6 and $C8^i$, corresponds to the direction of the long molecular axis. The line between C6 and C8 corresponds to the short molecular axis. The crystal structures of **1c**–**1f** and **2c**–**2f** are composed of two types of 2-D molecular arrangements, as shown in Figure 9. The first is

the J-aggregate-like 2-D stacking molecular layer. The second is the 2-D parallel molecular plane, in which the molecules are translated along both the long and short molecular axes. The intermolecular distances and angles between a reference molecule and three different types of neighbouring molecules were measured in each crystal structure (**1c**–**1f** and **2c**–**2f)** so as to characterise the 3-D crystal structures including the two types of the 2-D molecular arrangements. The three types of neighbouring molecules correspond to (i) an adjacent π-π stacked molecule, (ii) a molecule aligned along the long molecular axis, and (iii) a molecule aligned along the short molecular axis, with respect to the reference molecule, as shown in Figure 9. The type (i) and (ii) molecules were selected from the same J-aggregate like 2-D layer as the reference molecules, to evaluate the molecular arrangements in the 2-D layers. The type (iii) molecule was chosen from the adjacent 2-D layers to evaluate the structural relationships between the adjacent 2-D layers. The definition of the intermolecular distances and angles between the reference molecule and the three types of the neighbouring molecules is shown in Figure 10. The distance between the π-plane of a reference molecule and that of the adjacent π-π stacked type (i) molecule was measured and denoted as r_i. The intermolecular slip angles along the long molecular axis and the short molecular axis between a reference molecule and the type (i) molecule were estimated and denoted as θ_{i1} and θ_{i2}, respectively. The distance between the centroid of the reference molecule (Ce_r) and the centroid of molecule (ii) Ce_{ii} is denoted r_{ii}. θ_{ii} indicates an intermolecular angle between the reference molecule and molecule (ii), which was defined as an angle $\angle C6_r Ce_r Ce_{ii}$. The intermolecular distance r_{iii} and angle θ_{iii} between a reference molecule and the molecule (iii) were defined as a distance between Ce_r and Ce_{iii}, and the angle $\angle C6_r Ce_r Ce_{iii}$, respectively; note that only **2d** and **2**e have glide plane symmetry between the reference molecule and type (iii) molecule, yet their θ_{iii} values do not reflect this. This geometrical feature of the type (iii) molecules of **2d** and **2e** is intentionally distinguished from that of the other derivatives regardless of their θ_{iii} values. The measurements are listed in Table 3.

[Figure 8]

[Figure 9]

[Figure 10]

The relative arrangements of the reference molecules and type (i), (ii) and (iii) molecules in structures **1c**–**1f** and **2c**–**2f** are shown in Figures 11 and 12.

Table 3 lists the r_i and θ_{i1} values for **1c**–**1f** and **2c**–**2f**: they are all similar. The θ_{i2} value of **1e** (80°) was larger than the θ_{i2} values of the other derivatives. The θ_{i2} values of **1f** and **2f** (54° and 55°, respectively) were slightly smaller compared to **1c**, **1d** and **2c**–**2f** (60–67°). The arrangements of the reference molecules and the molecules (i) of **1e**, **2f** and **1c** are shown in Figure 11. **1e**, **1f** and **2f** have larger alkoxy substituents and had different θ_{i2} values to **1c**, **1d** and **2c**–**2f**. This difference indicates that the alkoxy substituents are the cause of the molecular distortion along the short molecular axis in the 1-D π-π stacked motif. However, we could not determine the effect of the terminal dialkyl substituents on the 1-D π-π stacked motif.

The θ_{ii}, r_{iii} and θ_{iii} values indicated the effects of the terminal dialkyl substituents on the arrangements of the molecules aligned along the long molecular axes and the short molecular axes of **1c**–**1f** and **2c**–**2f**. The structural relationships between the reference molecules, the molecules (ii) and the molecules (iii) of **1c**, **1e**, **1f**, **2c**, **2e** and **2f**

are described in Figure 12. The θ_{ii} values of **1c**–**1f** and **2f** (7–17°) were smaller than those of **2c**–**2e** (28–29°) and the r_{ii} values of **1c**–**1f** and **2f** (22.128–33.053 Å) were larger than those of **2c - 2e** (20.308–20.481 Å). These can be related to the location of the terminal dialkyl substituents and their effect on the intermolecular space between the reference molecule and type (ii) molecule. The terminal dialkyl substituents of type (ii) molecules in **1c**–**1f** and **2f** face those of the reference molecule, as shown in Figures 12(a), (b), (c) and (f). However, in **2c**–**2e** the terminal diethyl substituents of the type (ii) molecules face the alkoxy substituents of the reference molecules. Thus, the θ_{ii} values are larger because the dialkyl substituents occupy the intermolecular space between the reference molecules and type (ii) molecules, which also induced the small r_{ii} values, as shown in Figures 12(d) and (e). The exceptional large r_{ii} value of **1f** (33.053 Å) can be attributed to its decyloxy substituents penetrating into the intermolecular space between the reference molecule and type (ii) molecule, as shown in Figure 12(c). The r_{iii} values for **1c**–**1f** (11.021–13.589 Å), which have terminal dimethyl substituents, were smaller compared to **2c**–**2f** (14.347–15.58 Å). The θ_{iii} values of **1c**–**1f** (29–46°) were larger compared to **2c**–**2e** (21°). In **1c**–**1f**, the alkoxy substituents of the type (iii) molecules are located around the terminal dimethyl substituents of the reference molecules in the intermolecular space between molecules aligned along the short molecular axis, as shown in Figures 12(a), (b) and (c). In **2c**–**2e**, the spaces around the terminal amino groups are occupied by the larger diethyl substituents irrespective of the glide plane symmetry of **2d** and **2e**. The alkoxy substituents of **2c**–**2e** were located in the spaces around the cyano groups of the molecules aligned along the short molecular axes, as shown in Figures 12(d) and (e), this is related to the smaller θ_{iii} values. The decyloxy substituents line up and overlap in **2f** leading to a large spacing between adjacent molecules and, consequently, a large θ_{iii} value (88°), as shown in Figure 12(f).

A geometrical comparison of **1c**–**1f** and **2c**–**2f**, and the effects of the terminal dialkyl substituents on the molecular arrangement of the J-aggregate-like dye molecules is summarised in Figure 13. Three types of 1-D π-π stacking molecular arrangements along the short molecular axes were found in the crystal structures of **1c**–**1f** and **2c**–**2f**, as shown in Figure 13(a), (b) and (c). These three identified types have different intermolecular slip angles. The dialkyl substituents do not affect the molecule dislocation along the short molecular axis that is seen in the 1-D π-π stacked structures (**1c**–**1f** and **2c**–**2f**). The dialkyl substituents of **1c**–**1f** and **2f** face each other and align along the long molecular axis. This characteristic feature of J-aggregate-like 2-D arrangements is shown schematically in Figure 13(d) and (e–g). On the other hand, the terminal diethyl substituents of the molecules of **2c**–**2e** face the alkoxy substituents of the neighbouring molecules aligned along the long molecular axes. This induces a larger intermolecular angle between the molecules aligned along the long molecular axes in the J-aggregate-like 2-D layers of **2c**–**2e,** as shown in Figure 13(h). The structural relationships between the adjacent 2-D layers and the features of the 3-D molecular arrangement of **1c**–**1f** and **2c**–**2f** were categorised as shown in Figure 13(i), (j), (k), (l), (m) and (n) according to their r_{iii} and θ_{iii} values. In **1c**–**1f** and **2f** the most important factor influencing the molecular distortions along the short molecular axis between the stacked 2-D layers shown in Figure 13(o), (p), (q) and (r) was the location of the terminal dialkyl substituents. Their position affected the intermolecular space between molecules aligned along their long molecular axis. In **2c**–**2e** the diethyl substituents face the alkoxy substituents. The stacking direction was almost normal to the molecular π-planes, as shown in Figure 13(s) and (t).

[Table 3]

[Figure 11]

[Figure 12]

[Figure 13]

3.3. Lattice energy calculations for the DMA and the DEA derivatives

Lattice energy calculations were carried out to interpret the effects of the terminal dimethyl and the diethyl substituents on the molecular arrangements of **1c**–**1f** and **2c**–**2f** from an energetic perspective. The calculations indicate the importance of the strong intermolecular interactions that stabilise the lattice, as listed in Table 4.

The strong contribution to the lattice energy of the π-π stacked molecular pairs (previously described as type (i) molecules) was calculated for all the dye-derivatives. This 1-D π-π stacking arrangement that is observed in **1c**–**1f** and **2c**–**2f** was found to play a significant role in the crystal packing of this dye system, regardless of the different substituents and the slightly different intermolecular slip angles.

For structures **1d**–**1f** and **2f**, the third and fourth energetic contributions were calculated for the adjacent molecules that were aligned along the short molecular axes and the molecular stacking directions from the reference molecule. These third and fourth contributors to the lattice energy for **1d**–**1f** and **2f** derive from the adjacent 2-D layers, which do not include the reference molecule. On the other hand, the third and the fourth energetic contributors in **1c** and **2c**–**2e** were the molecules aligned along the long molecular axes and in the molecular stacking direction from the reference molecules, belonging to the 2-D layer including the reference molecules. In the crystal structures of **2c**–**2e**, the dye molecules are aligned along the long molecular axis and the diethyl substituents face towards the alkoxy substituents of the adjacent molecules. This arrangement of substituents that leads to the large θ_{ii} values (28–29°) and the small r_{ii} values (20.308–20.481 Å) of **2c**–**2e** contributed to the overlap between the molecules aligned along the long molecular axes and that overlap in the molecular stacking direction, as shown in Figure 13(h). This molecular overlap in the crystal structures of **2c**–**2e** caused strong energetic interactions between the molecules belonging to the same 2-D layers. The value of θ_{ii} in **1c** (17°) was smaller than in **2c**–**2e**, but larger than in **1d**–**1f** and **2f**. As listed in Table S3, the fifth and six energetic contributions in **1c** were due to the molecules aligned along the short molecular axis and the molecular stacking direction. The energy gap between the third and fourth contributions and the fifth and sixth contributions in **1c** was the smallest (− 6.9 kJ·mol^{-1}, 1.4% of the total lattice energy) compared with the energy gaps of **1d**–**1f** and **2c**–**2f** as shown in Table S3. Therefore, **1c** could be regarded as a molecule with intermediate energetic properties between **1d**–**1f, 2f** and **2c**–**2e**. The large energy gap between the third and fourth contributions and the fifth and sixth contributions of **2c**–**2e** indicates that the 2-D layers play a significant role in the crystal packing of structures **2c**–**2e**. The lattice energy calculations indicate that the 1-D π-π stacked molecules are important for the formation of the crystal structures of **1c**–**1f** and **2c**–**2f,** irrespective of the different substituents. The crystal packing of **1c**–**1f** and **2c**–**2f** was affected by the location of the dialkyl substituents with respect to the intermolecular space between 1-D π-π stacked molecules. Their location affected the relative arrangement of molecules and, thus, the crystal packing.

[Table 4]

4. Conclusions

Five alkoxylated bisazomethine derivatives with dimethyl substituents on the terminal amino groups were found to form crystal structures with characteristic J-aggregate-like 2-D molecular arrangements. In contrast, a phenoxylated derivative with dimethyl substituents formed a herringbone crystal structure that did not include the J-aggregate-like 2-D arrangement. Viewing the 2-D layers of the five derivatives from the direction of the long molecular axes, the molecules forming the 2-D layers were slightly slipped in the direction of the short molecular axes. This molecular dislocation along the short molecular axes in the 2-D layers is similar to that of the reported crystal structures of the decyloxylated bisazomethine derivatives that have diethyl substituents on the terminal amino group. This slipped geometry was different from the structural features of the J-aggregate-like 2-D layers of the other eight alkoxylated bisazomethine derivatives with diethyl substituents.

The geometrical comparisons and lattice energy calculations with respect to the crystal structures of each of the 4 alkoxylated bisazomethine derivatives that have dimethyl and diethyl substituents on the terminal amino groups indicate that the terminal dialkyl substituents did not affect the 1-D arrangements of the π-π stacking molecules in this dye system. However, the terminal dialkyl substituents did affect the arrangement of the molecules aligned along the long molecular axes and the short molecular axes, leading to the different structural features of the J-aggregate like 2-D molecular arrangements and the 3-D crystal structures of the derivatives. This result demonstrates that substitutions at the terminal amino groups can be used to modify the molecular arrangements and can be used in the design of low-dimensional materials that could have applications in optoelectronic devices. Further investigations, which involve spectroscopic analyses and theoretical calculations, will investigate the electronic properties and further investigate the molecular arrangements in the solid state of this dye system.

Acknowledgement

The authors are grateful to Dr. Hiroyasu Sato (Rigaku) for his kind and expeditious support in the X-ray diffraction re-measurement with its analysis on **1f** and the re-refinement on the crystal structures of **1a** and **1c**.

References

1 A. Gretchikhine, G. Schweitzer, M. Van der Auweraer, R. De Keyzer, D. Vandenbroucke and F .C. De Schryver, *J. Appl. Phys.*, 1999, **85**, 1283–1293.

2 T. Kobayashi, *J-aggregates*, World Scientific Publishing, Singapore, 1996.

3 Y. Wang, *J. Opt. Soc. Am. B*, 1991, **8**, 981–985.

4 F. C. Spano and S. Mukamel, Phys. Rev. A, 1989, **40**, 5783–5801.

5 J. Moll, S. Daehne, J. R. Durrant and D. A. Wiersma, J. Chem. Phys., 1995, **102**, 6362–6370.

6 S. Tatsuura, M. Tian, M. Furuki, Y. Sato, L. S. Pu and O. Wada, *Jpn. J. Appl. Phys.*, 2000, **39**, 4782.

7 M. Kasha, *Spectroscopy of the Excited State* (ed. by B. D. Bartolo), Plenum Press, 337, 1976.

8 G. Scheibe, *Angew. Chem.*, 1939, **52**, 631–637.

9 A. S. Davydov, *Theory of Molecular Exitons*, McGraw-Hill, New York, 1962.

10 V. Czikkely, H. D. Forsterling and H. Kuhn, *Chem. Phys. Lett.*, 1970, **6**, 11–14.

11 D. L. Smith, *Photogr. Sci. Eng.*, 1974, **18**, 309–322.

12 S. Kirstein, R. Steitz, R. Garbella, and H. Möhwald, *Photogr. Sci. Eng.*, 1973, **17**, 34–342.

13 K. Nakatsu, H. Yoshioka and S. Nishigaki, *Nihon Shashin Gkkai-shi* (in Japanese), 1983, **46**, 89–98.

14 H. Kuhn and C. Kuhn, *J-aggregates* (ed. by T. Kobayashi), World Scientific Publishing, Singapore, 1, 1996.

15 H. Yao, M. Omizo and N. Kitamura, *Chem. Commun.*, 2000, **9**, 739–740.

16 N. Kato, K. Yuasa, T. Araki, I. Hirosawa, M. Sato, N. Ikeda, K. I. Iimura and U. Uesu, *Phys. Rev. Lett.*, 2005, **94**, 136404.1–136404.4.

17 K. H. Kim, S. Y. Bae, Y. S. Kim, J. A. Hur, M. H. Hoang, T. W. Lee, M. J. Cho, Y. Kim, M. Kim, J. I. Jin, S. J. Kim, K. Lee, S. J. Lee and D. H. Choi, *Adv. Mater*., 2011, **23**, 3095–3099.

18 S. Matsumoto, E. Horiguchi-Babamoto, R. Eto, S. Sato, T. Kobayashi, H. Naito, M. Shiro and H. Takahadhi, *Dyes Pigm.*, 2012, **90**, 431–435.

19 S. Matsumoto, T. Kobayashi, T. Aoyama and T. Wada, *Chem. Commun.*, 2003, 1910–1911.

20 T. Kobayashi, S. Matsumoto, T. Tanaka, H. Kunugita, K. Ema, T. Aoyama and T. Wada, *Phys. Chem. Chem. Phys*., 2005, **7**, 1726–1731.

21 T. Kobayashi, S. Matsumoto, T. Aoyama and T. Wada, *Thin Solid Films*, 2006, **509**, 145–148.

22 T. Hosokai, S. Kera, K. K. Okudaira, N. Ueno and S. Matsumoto, *Mol. Cryst. Liq. Cryst*., 2007, **472**, 43–50.

23 T. Hosokai, T. Aoyama, T. Kobayashi, A. Nakao and S. Matsumoto, *Chem. Phys. Lett*., 2010, **487**, 77–80.

24 T. Tanaka, M. Satoh, M. Ishitobi, T. Aoyama and S. Matsumoto, *Chem. Lett.*, 2011, **40**, 1170–1172.

25 T. Tanaka, S. Matsumoto, T. Kobayashi, M. Satoh and T. Aoyama, *J. Phys. Chem*., 2011, **115**, 19598–19605.

26 J. C. Ribierre, M. Sato, A. Ishizuka, T. Tanaka, S. Watanabe, M. Matsumoto, S. Matsumoto, M. Uchiyama and T. Aoyama, *Org. Electron.,* 2012, **12**, 999-1003.

27 S. Matsumoto, M. Satoh, D. Tsuchida, T. Kobayashi, T. Aoyama and T. Wada, *Trans. MRS-J*, 2005, **30**, 345–348.

28 B. S. Kim, D. Kashibuchi, Y. A. Son, S. H. Kim and S. Matsumoto, *Dyes Pigm*., 2011, **90**, 56–64.

29 K. Kinashi, K. P. Lee, S. Matsumoto, K. Ishida and Y. Ueda, *Dyes Pigm.*, 2011, **92**, 783–788.

30 B. S. Kim, T. Jindo, R. Eto, Y. Shinohara, Y. A. Son, S. H. Kim and S. Matsumoto, *CrystEngComm*., 2011, **13**, 5374–5383.

31 N. Sasaki, B. S. Kim, Y. A. Son, S. H. Kim and S. Matsumoto, *in preparation*.

32 K. Shirai, M. Matsuoka, K. Fukunishi, *Dyes Pigm.*, 2000, **47**, 107–115.

33 S. Matsumoto, K. Shirai, K. Kobayashi, T. Wada and M. Shiro, *Z. Kristallogr*., 2004, **219**, 239–243.

34 S. H. Kim and S. Matsumoto, *Dyes Pigm.*, 2007, **73**, 406–408.

35 Y. A. Son, S. Matsumoto, E. Mi. Han, S. Wang and S. H. Kim, *Mol. Cryst. Liq. Cryst*., 2008, **492**, 46–55.

36 J. Mei, Y. Diao, A. L. Appleton, L. Fang and Z. Bao, *J. Am. Chem. Soc*., 2013, **135**, 6724–6746.

37 R. H. Kim, H. J. Kim, I. Bae, S. K. Hwang, D. B. Velusamy, S. M. Cho, K. Takaishi, T. Muto, D. Hashizume, M. Uchiyama, P. Andre, F. Mathevet, B. Heinrich, T. Aoyama, D. E. Kim, H. Lee, J. C. Ribierre and C. Park, *Nat. Commun.*, 2014, **5**, 3583–3595.

38 H. Minemawari, T. Yamada, H. Matsui, J. Tsutsumi, S. Haas, R. Chiba, R. Kumai, T. Hasegawa, *Nature*, 2011,

475, 364–367.

39 M. C. Burla, R. Caliandro, M. Camalli, B. Carrozzini, G. L. Cascarano, L. D. Caro, C. Giacovazzo, G. Polidori and R. Spagna, *J. Appl. Crystallogr.*, 2005, **38**, 381–388.

40 G. M. Sheldrick, 2014, *Acta Cryst.*, **A70**, C1437.

41 CrystalStructure 4.0: Crystal Structure Analysis Package, Rigaku Corporation (2000–2010), Tokyo 196–8666, Japan.

42 CrystalStructure 4.2: Crystal Structure Analysis Package, Rigaku Corporation (2000-2015). Tokyo 196-8666, Japan.

43 C. F. Macrae, I. J. Bruno, J. A. Chisholm, P. R. Edgington, P. McCabe, E. Pidcock, L. Rodriguez-Monge, R. Taylor, J. van de Streek and P. A. Wood, *J. Appl. Cryst.*, 2008, **41**, 466–470.

44 A. Gavezzotti, *Z. Kristallogr.*, 2005, **220**, 499–510.

45 A. Gavezzotti, OPiX: a Computer Program Package for the Calculation of Intermolecular Interactions and Crystal Energies, University of Milan, Milan, Italy, 2003.

46 F. H. Allen, O. Kennard, D. G. Watson, L. Brammer, A. G. Orpen and R. Taylor, *J. Chem. Soc.*, *Perkin Trans.* ***2***, 1987, S1–S19.

47 G.Fillippini and A. Gavezzotti, *Acta. Crystal.*, 1993, **B49**, 868-880.

48 A. Gavessotti and G. Filippini, Energetic aspects of crystal packing: experiment and computer simulations, in *Theoretical Aspects and Computer Modeling of the Molecular Solid State*, ed. A. Gavezzotti, Wiley & Sons, Chichester, 1997.

49 The energetic functional form for the *i-j* atom-atom potential in the OPiX code is: E (*ij*, kJ mol^{-1}) = A exp(–BR_{ij}) – CR_{ij}^{-6} + q_iq_j/R_{ij}, where R_{ij} is distances between the atomic nuclear positions of atoms *i* and *j*; A, B and C are empirical parameters; and q_i and q_j are atomic charge parameters located at atomic nuclear positions of atoms *i* and *j*. The total lattice energy is summed pairwise over atoms in the unit cell. The output from the calculations yields the total lattice energy and the energetic contributions of molecular pairs to the total lattice energy.

50 A. Nangia, *Acc. Chem. Res.*, 2008, **41**, 595–604.

51 A. I. Kitaigorodsky, *Molecular Crystals and Molecules*, Academic Press, New York, 1973.

52 G. R. Desiraju, J. J. Vittal and A. Ramanan, *Crystal Engineering*, World Scientific Publishing, Singapore, 2011.

Figure and Table captions

Figure 1 The features of the reported crystal structures of the DEA derivatives:[31,34] (a) chemical structures of the DEA derivatives, (b) the J-aggregate-like 2-D molecular arrangement of the DEA derivatives, the features of the 3-D crystal structures of (c) the octoxylated and (d) the decyloxylated derivatives, respectively.

Figure 2 Chemical structures of the six DMA derivatives (**1a**–**1f**) and the four DEA derivatives (**2c**–**2f**).

Figure 3 Molecular geometries (ORTEP) drawn with 30% probability; H atoms are omitted for clarity: (a) **1a**, (b) **1c**, (c) **1e** and (d) **1f**.

Figure 4 Crystal structure of **1a**: (a) the molecular arrangement in the (400) plane, (b) looking down the [010] direction, and (c) looking down the [001] direction, respectively.

Figure 5 Crystal structure of **1c**: (a) the molecular arrangement in the (010) plane, (b) looking down parallel to the (010) plane from the direction of the long molecular axis, and (c) looking down parallel to the (010) plane from the molecular stacking direction, respectively.

Figure 6 Crystal structure of **1e**: (a) the molecular arrangement on the (001) plane, (b) looking down in parallel with the (001) plane from the direction of the long molecular axis, and (c) looking down in parallel with the (001) plane from the molecular stacking direction, respectively.

Figure 7 Crystal structure of **1f**: (a) the molecular arrangement in the (01-1) plane, (b) looking down parallel to the (01-1) plane from the direction of the long molecular axis, and (c) looking down parallel to the (01-1) plane from the molecular stacking direction, respectively.

Figure 8 The geometrical points on the π-conjugated system for the evaluation of the molecular arrangements of **1c**–**1f** and **2c**–**2f**: (a) the positions of the carbon atoms, C6, C8, $C6^{i}$ and $C8^{i}$, depicted by ORTEP drawing, (b) the geometrical standards on the π-conjugated system drawn by Mercury 3.1, respectively.

Figure 9 The features of the molecular arrangement of **1c**–**1f** and **2c**–**2f** and the three types of the neighbouring molecules selected for the geometrical measurements; the red-coloured molecule is a reference molecule, (i) the blue-coloured molecule is an adjacent π-π stacking molecule, (ii) the green-coloured molecule is a molecule aligned along the long molecular axis, and (iii) the yellow-coloured molecule is a molecule aligned along the short molecular axis, respectively.

Figure 10 The definition of the distances and angles between a reference molecule and the three types of the neighbouring molecules: (a) the definition of the distances and angles between a reference molecule and a type (i) molecule, (b) the definition of the distances and angles between a reference molecule and the type (ii) and type (iii) molecules, respectively.

Figure 11 The 1-D π–π stacking molecular arrangements of: (a) **1**, (b) **2f** and (c) **1c**, respectively.

Figure 12 The arrangements of the molecules aligned along the long molecular axis (ii) and the short molecular axis (iii) in: (a) **1c**, (b) **1e**, (c) **1f**, (d) **2c**, (e) **2e** and (f) **2f**, respectively.

Figure 13 The structural features of the molecular arrangements of **1c**–**1f** and **2c**–**2f**. The features of the 1-D stacking molecular arrangements of; (a) **1e**, (b) **1f** and **2f**, and (c) **1c**, **1d** and **2c**–**2e**. The features of the J-aggregate like 2-D molecular arrangements of; (d) **1e**, (e) **1f**, (f) **2f**, (g) **1c** and **1d**, and (h) **2c**–**2e**. The features of the 3-D molecular arrangements of; (i) **1e**, (j) **1f**, (k) **2f**, (l) **1c** and **1d**, (m) **2c**, and (n) **2d** and **2e**. The 3-D crystal structures of (o) **1e**, (p) **1f**, (q) **2f**, (r) **1c**, (s) **2c** and (t) **2d**.

Table 1 Crystallographic and structural refinement data of **1a - 1f** and **2c - 2f**.

Table 2 Interlayer distances between the adjacent 2-D layers in **1a**–**1f**.

Table 3 The results of the geometrical analysis.

Table 4 Results of the lattice energy calculations on **1c**–**1f** and **2c**–**2f**.

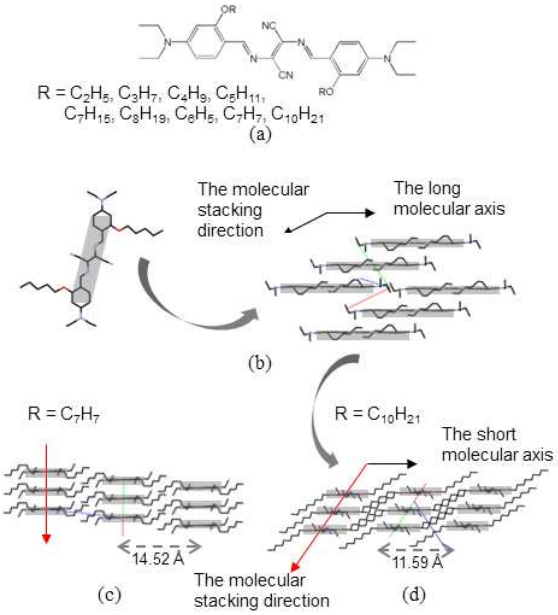

Figure 1

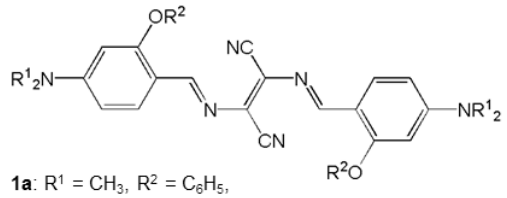

1a: $R^1 = CH_3$, $R^2 = C_6H_5$,
1b: $R^1 = CH_3$, $R^2 = CH_3$,
1c: $R^1 = CH_3$, $R^2 = C_3H_7$,
1d: $R^1 = CH_3$, $R^2 = C_4H_9$,
1e: $R^1 = CH_3$, $R^2 = C_5H_{11}$,
1f: $R^1 = CH_3$, $R^2 = C_{10}H_{21}$,
2c: $R^1 = C_2H_5$, $R^2 = C_3H_7$,
2d: $R^1 = C_2H_5$, $R^2 = C_4H_9$,
2e: $R^1 = C_2H_5$, $R^2 = C_5H_{11}$,
2f: $R^1 = C_2H_5$, $R^2 = C_{10}H_{21}$,

Figure 2

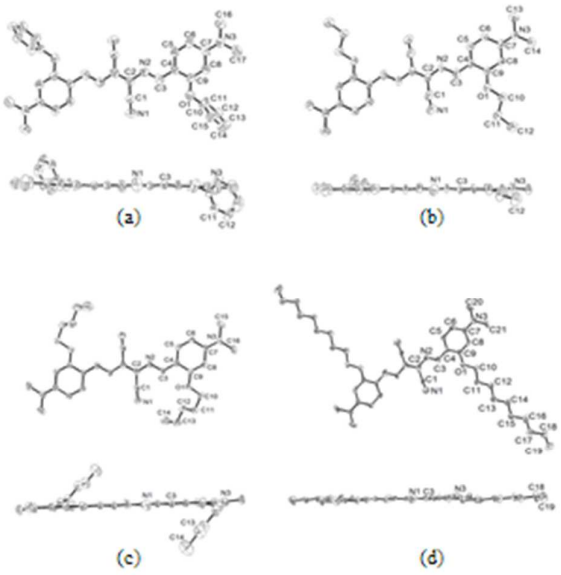

Figure 3

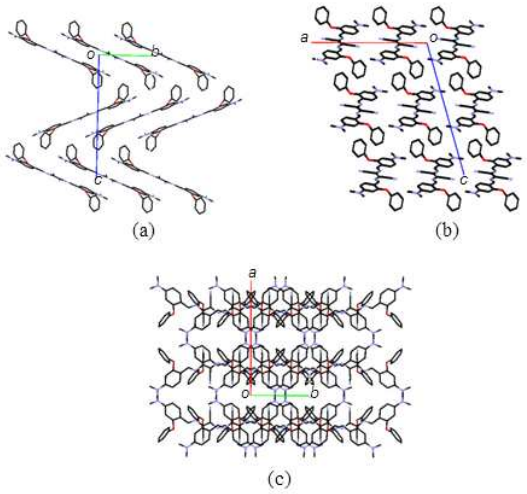

Figure 4

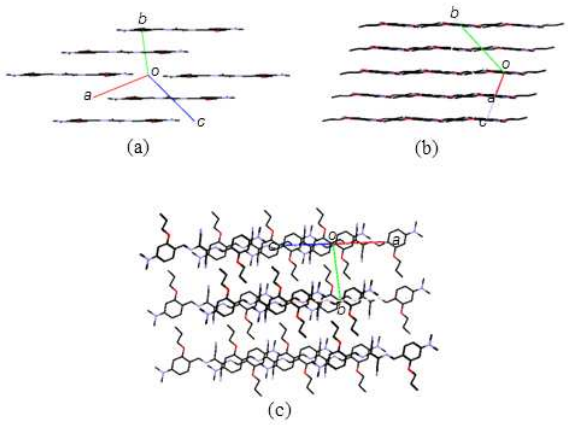

Figure 5

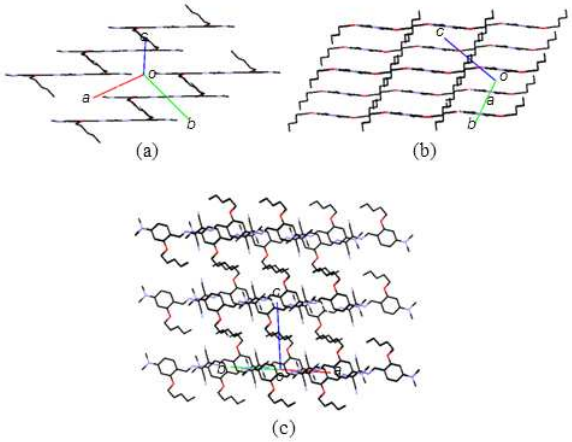

Figure 6

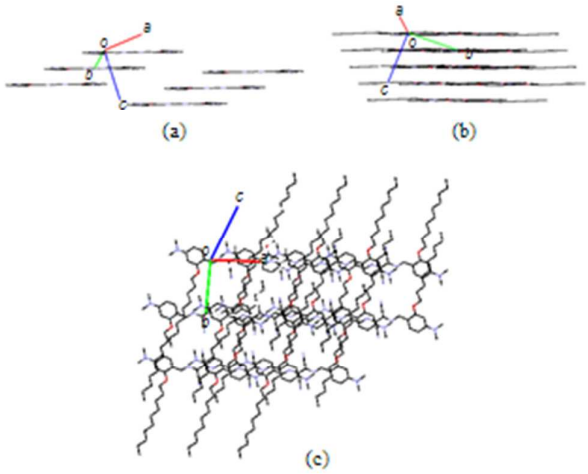

Figure 7

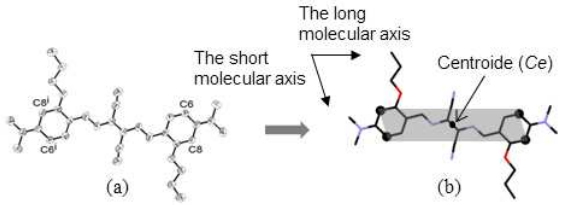

Figure 8

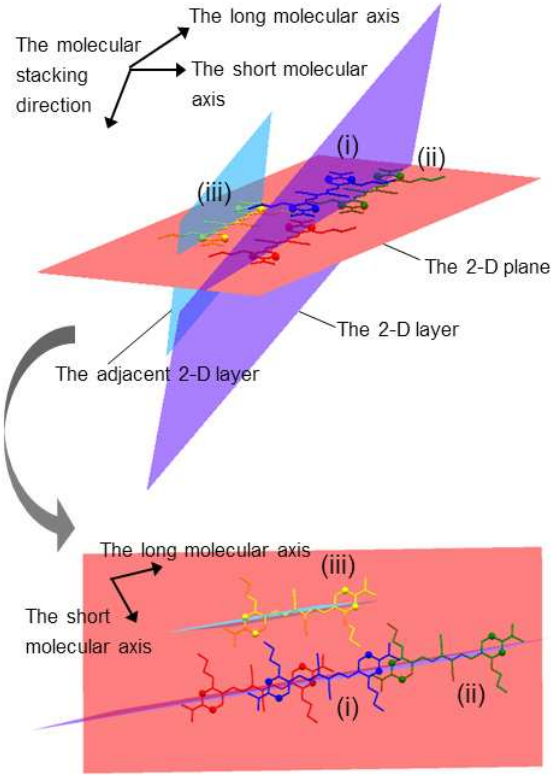

Figure 9

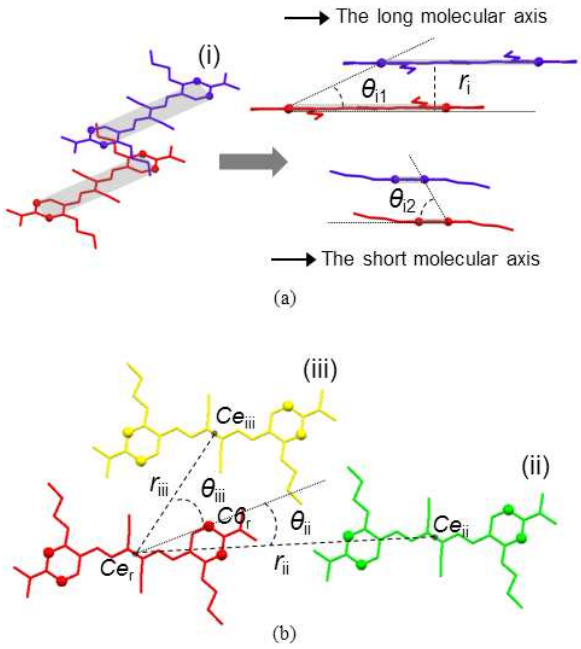

Figure 10

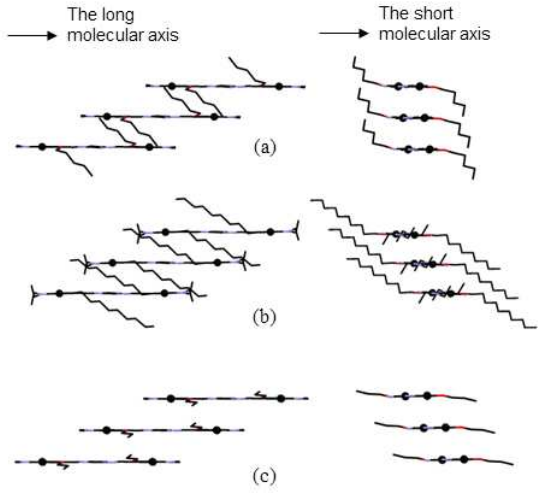

Figure 11

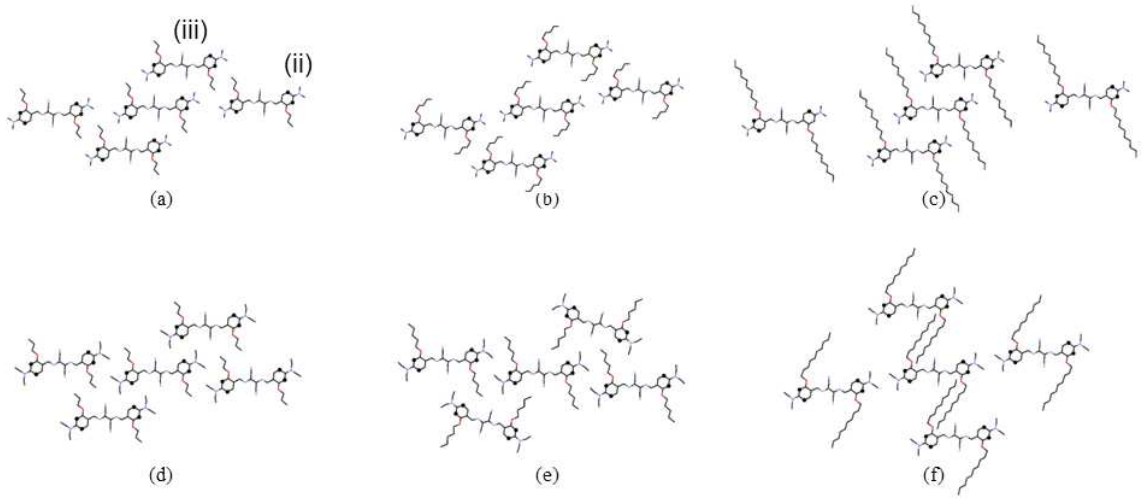

Figure 12

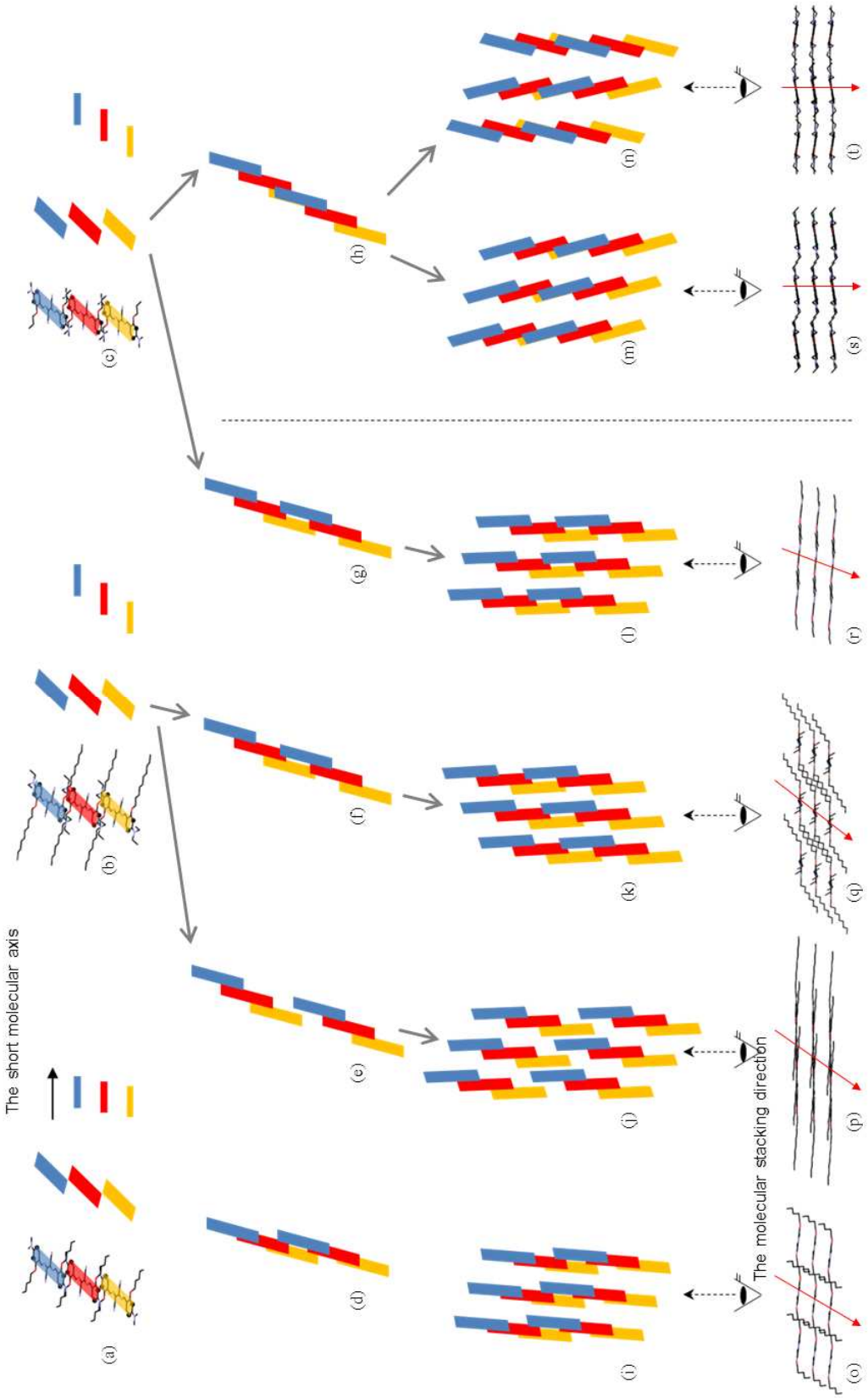

Figure 13

Table 1

Crystal data	**1a**	**1b**	**1c**	**1d**	**1e**	**1f**	**2c**[a]	**2d**[b]	**2e**[a]	**2f**[a]
Crystal size/mm	0.30, 0.04, 0.04	0.15, 0.10, 0.08	0.20, 0.04, 0.04	0.10, 0.08, 0.06	0.60, 0.08, 0.08	0.40, 0.08, 0.04	0.15, 0.10, 0.08	0.30, 0.10, 0.02	0.20, 0.10, 0.04	0.50, 0.10, 0.10
Chemical formula	$C_{34}H_{30}N_6O_2$	$C_{24}H_{26}N_6O_2$	$C_{28}H_{34}N_6O_2$	$C_{30}H_{38}N_6O_2$	$C_{32}H_{42}N_6O_2$	$C_{42}H_{62}N_6O_2$	$C_{32}H_{42}N_6O_2$	$C_{34}H_{46}N_6O_2$	$C_{36}H_{50}N_6O_2$	$C_{46}H_{70}N_6O_2$
Formular weight/g mol^{-1}	554.65	430.51	486.62	514.67	542.72	682.99	542.72	570.78	598.83	739.1
Temperature/ K	296	296	296	296	296	93	296.1	296.1	296.1	296.1
Crystal system	monoclinic	triclinic	triclinic	triclinic	triclinic	triclinic	triclinic	monoclinic	monoclinic	triclinic
Space group	*C*2/c	*P*-1	*P*-1	*P*-1	*P*-1	*P*-1	*P*-1	$P2_1/c$	$P2_1/a$	*P*-1
a/ Å	17.6278(7)	7.47796(15)	8.7038(4)	8.5720(2)	8.4017(2)	8.6252(3)	8.2371(4)	8.624(3)	8.2480(3)	8.1175(3)
b / Å	8.6461(4)	8.79150(16)	9.2191(5)	9.4914(3)	10.0488(2)	10.9509(5)	8.8466(4)	22.721(6)	23.4817(7)	12.4218(4)
c / Å	21.0723(8)	10.00729(18)	10.0892(5)	10.6283(3)	10.0892(5)	11.5620(7)	11.2530(5)	8.511(2)	9.0521(3)	13.0984(4)
α / °	90	67.6476(10)	110.554(3)	115.2669(12)	95.1228(12)	94.067(4)	89.726(3)	90	90	62.610(2)
β / °	105.829(19)	72.0277(10)	110.343(3)	98.1638(14)	102.0454(13)	93.088(4)	70.242(2)	81.66(3)	94.551(2)	86.305(2)
γ / °	90	80.1605(10)	97.368(3)	102.7069(14)	108.3491(12)	112.605(4)	83.791(3)	90	90	76.962(2)
V / Å^3	3089.9(2)	577.71(2)	681.26(6)	735.06(4)	779.60(4)	1001.74(9)	766.77(6)	1649.5(8)	1747.66(9)	1141.29(6)
Z	4	1	1	1	1	1	1	2	2	1
D_x/ g cm^{-3}	1.192	1.237	1.186	1.163	1.156	1.132	1.175	1.149	1.138	1.075
μ / mm^{-1}	0.612	0.662	0.615	0.595	0.584	0.546	0.594	0.574	0.563	0.511
F (000)	1168	228	260	276	292	372	292	616	648	404
T_{min}	0.752	0.801	0.547	0.840	0.674	0.420	0.776	0.569	0.762	0.747
T_{max}	0.976	0.948	0.976	0.965	0.954	0.995	0.954	0.989	0.956	0.950
No. of reflection measured	13570	5395	6311	7020	7416	14895	7142	11 646	16 246	10398
No. of unique reflections	2553	1973	2333	2516	2671	4000	2639	2798	3053	3896
No. of parameters	192	145	166	172	181	229	181	213	224	279
θ_{max}/ °	64.996	68.25	68.231	68.16	68.21	75.452	68.19	68.23	68.20	68.16
R 1, *wR*,	0.1116, 0.2090	0.0565, 0.1959	0.0987, 0.3459	0.0619, 0.2556	0.0566, 0.1945	0.0652, 0.1656	0.0762, 0.2816	0.0527, 0.1197	0.0527, 0.0794	0.0693, 0.0932
GOF	1.212	1.061	0.879	1.134	1.110	1.036	1.201	1.175	1.214	1.383
$\Delta\rho_{max}$, $\Delta\rho_{min}$/ e Å^{-3}	0.20, -0.21	0.19, -0.24	0.24, -0.22	0.36, -0.21	0.21, -0.23	0.20, -0.26	0.36, -0.30	0.65, -0.72	0.25, -0.24	0.34, -0.46

[a] CSD code of **2c**, **2e** and **2f** are UXIBEJ, UXIBIN and UXICAG, respectively. [30] [b] Crsytal structure of **2d** have been reported previously. [35]

Table 2

	1a	1b	1c	1d	1e	1f
The interlayer distances between the adjacent 2-D layers/ Å	-	6.17	8.56	8.28	10.00	8.11

Table 3

	1c	1d	1e	1f	2c[a]	2d[b]	2e[a]	2f[a]
(i)								
r_i/ Å	3.39	3.44	3.40	3.29	3.53	3.52	3.64	3.42
θ_{i1}/ °	26	26	25	26	26	27	26	29
θ_{i2}/ °	60	67	80	55	64	63	63	54
(ii)								
r_{ii}/ Å	22.95(1)	24.357(5)	22.128(4)	33.053(3)	20.308(6)	20.31(1)	20.481(3)	22.558(3)
θ_{ii}/ °	17	15	7	16	28	28	29	10
(iii)								
r_{iii}/ Å	11.021(9)	12.671(5)	13.589(3)	11.032(2)	14.347(6)	15.23[c]	15.58[c]	14.501(2)
θ_{iii}/ °	36	29	46	36	21	21[c]	21[c]	88

[a, b] The crystal structures of **2c** - **2f** have been reported previously. [30,35] [c] **2d** and **2e** have glide plane symmetry between the reference molecules and the molecules (iii).

Table 4

		Contribution of molecular pairs to the total lattice energies			
	Total lattice enegy/ kJ mol^{-1}	1st and 2nd contributions/ kJ mol^{-1} (ratio, ADC)		3rd and 4th contributions/ kJ mol^{-1} (ratio, ADC)	
1c	-508.0	-115.1	(22.7%, 45501 and 65501)	-47.2	(9.3%, 45601 and 65401)
1d	-528.2	-118.7	(22.5%, 45501 and 65501)	-50.2	(9.5%, 44501 and 66501)
1e	-537.3	-127.4	(23.7%, 45501 and 65501)	-49.5	(9.2%, 45401 and 65601)
1f	-706.9	-116.3	(16.5%, 45501 and 65501)	-64.7	(9.2%, 54501 and 56501)
2c[a]	-574.4	-120.0	(20.9%, 54501 and 56501)	-86.5	(15.1%, 44501 and 66501)
2d	-592.9	-123.3	(20.8%, 45501 and 65501)	-85.9	(14.5%, 45401 and 65601)
2e[a]	-596.4	-116.9	(19.6%, 55401 and 55601)	-88.6	(14.9%, 45601 and 65401)
2f[a]	-724.1	-140.4	(19.4%, 45501 and 65501)	-62.6	(8.6%, 46401 and 64601)

[a] The results of the lattice energy calculations of **2c**, **2e** and **2f** have been reported previously.[30]